Norwegian University of
Science and Technology

Investigation of Pulsed Laser Deposition Growth Parameters and their influence on the Sheet Resistance of a Complex Oxide Heterointerface

Filip Dovland

Master of Science in Electronics
Submission date: July 2011
Supervisor: Thomas Tybell, IET

Norwegian University of Science and Technology
Department of Electronics and Telecommunications

Problembeskrivelse

Student: Filip Dovland

Tittel: Investigation of Pulsed Laser Deposition Growth Parameters and their influence on the Sheet Resistance of a Complex Oxide Heterointerface

Problem: Functional interfaces have recently raised large interest. In order to optimize the functional properties of the interfaces, a high degree of control is important. In this master project the goal is to investigate how pulsed laser deposition can be used to tailor the interface between LaAlO3 and SrTiO3, and how the growth parameters affect the conductivity of that interface. It is a sub-goal to elucidate if the conductivity along the interface is anisotropic along the <100> and <010> directions of the interface surface.

Veileder: Jos Emiel Boschker
Faglærer: Thomas Tybell

Abstract

In this project, the growth parameters of Pulsed Laser Deposition are optimized in order to obtain a high quality interface between two complex oxides, $LaAlO_3$ and $SrTiO_3$. The prepared samples are compared by their sheet resistance, and the influence by the various growth parameters are investigated. The main finding is that reducing the laser fluence significantly lowers the sheet resistance. The lowest obtained sheet resistance was 81.2kΩ. This value was obtained with a laser fluence of 0.7 J/cm^2 and the results indicate that more can be gained by going even lower.

In previous work, a strong anisotropy of the sheet resistance has been observed. The anisotropy is further studied in this project and compared with the step–and–terrace topography at the interface. Atomic Force Microscopy is used to obtain the step directions and terrace widths, and these values are compared with resistance measurements. No correlation is found between these data. The results suggests that the anisotropy is due to other factors than the steps–and–terraces.

Contents

1 Introduction **1**

2 Background **3**
2.1 Materials . . . 3
2.1.1 Perovskite oxides . . . 3
2.1.2 The LAO/STO interface . . . 4
2.1.3 Step–and-terrace surface . . . 4
2.2 Interface properties . . . 5
2.3 Modelling the interface . . . 5
2.3.1 Electronic reconstruction . . . 5
2.3.2 Criticism to electronic reconstruction . . . 6
2.3.3 La doping . . . 8
2.3.4 Oxygen vacancies . . . 8
2.4 Introduction to thin film growth with PLD . . . 9
2.5 Summary . . . 11

3 Experimental **13**
3.1 The sample creation process . . . 13
3.1.1 Preparing the substrate for PLD growth . . . 13
3.1.2 Thin film growth with PLD . . . 13
3.1.3 Creating electrical contact to the interface . . . 14
3.2 Characterization . . . 17
3.2.1 Tuning growth parameters . . . 17
3.2.2 Examining surface topography with AFM . . . 21
3.2.3 Sheet resistance measurements . . . 22
3.2.4 Contact characterization . . . 24
3.2.5 Growth monitoring with RHEED . . . 25
3.2.6 Crystal quality verification with XRD . . . 27
3.3 Summary . . . 27

4 Results **29**
4.1 Contacts . . . 29
4.2 Sheet resistance and the effect of growth parameters . . . 32
4.3 Anisotropic resistance . . . 35

5 Discussion **37**
5.1 Contacts 37
5.2 Influence of growth parameters 38
5.3 Anisotropic resistance 40

6 Conclusion **43**

A Matlab scripts **44**

Acronyms

2DEG Two–dimensional Electron Gas.

AFM Atomic Force Microscopy.

HEMT High Electron Mobility Transistor.

LAO $LaAlO_3$.

MOSFET Metal–Oxide–Semiconductor Field–Effect–Transistor.

PCB Printed Circuit Board.

PLD Pulsed Laser Deposition.

PVD Physical Vapor Deposition.

RHEED Reflection High Energy Electron Diffraction.

STO $SrTiO_3$.

TLM Transmission Line Measurement.

XRD X–Ray Diffraction.

1 Introduction

The study of the boundary between different perovskite oxides is a rapidly increasing research field. In recent years it has become possible to synthesize and study atomically sharp heterointerfaces of these materials [1]. It is possible to engineer interfaces that don't naturally occur in nature and thus obtain material properties which are beyond what can be achieved in the bulk materials [2].

In semiconductor devices, heterointerfaces are becoming progressively more important. In his Nobel Lecture in 2000, Herbert Kroemer said that "The interface is the device" [3]. This statement is becoming increasingly accurate as the dimensions are being reduced down to the nanometer scale. Precise control over the interface is required to manufacture devices at this scale [4].

Perovskite oxides is a class of materials with a wide range of interesting material properties. Among the fascinating phenomena observed in these materials are high–T_c superconductivity and colossal magnetoresistance [5].

The ability to combine these materials with atomic level precision, opens a new world of structural and functional properties. One such interface which has gained much interest in recent years, is the interface between $LaAlO_3$ (LAO) and $SrTiO_3$ (STO). In 2004 Ohtomo and Hwang demonstrated that the interface between these two materials is conducting, even though both materials themselves are insulators [6]. Since then, many fascinating phenomena have been demonstrated for this interface, including both superconductuctivity and magnetoresistivity [7, 8].

The development of Pulsed Laser Deposition (PLD) has made a vital improvement to the study of oxide heterointerfaces. Oxides have traditionally been far more difficult to grow than semiconductors. With todays PLD systems, researches create oxide interfaces which rival semiconductors in both abruptness and crystalline perfection [5]. The method's relatively cheap and simple implementation is another reason why it has gained such popularity [9].

Although the setup of a PLD system is simple, the growth process itself is not. The growth is characterized by many complex processes including ablation, adsorption and nucleation [9]. Moreover, different groups report growth with significantly different growth parameters, but little has been published about how these parameters affect the interface (apart from the oxygen pressure) [6, 7, 10].

In this project, LAO/STO interfaces will be grown with PLD while tuning the various growth parameters. These parameters and their effect on the interface quality will be analyzed and compared.

Electrical contacts to this kind of interface has received little attention in

literature. In earlier work, contacts to the LAO/STO interface has been demonstrated by a manual method [11]. However, the contacts had large, and varying contact areas and ill–defined contact resistances. This project aims at developing a method to create a well–defined and reproducible contact pattern.

2 Background

A Two–dimensional Electron Gas (2DEG) is a gas of electrons which can only move in two dimensions. 2DEGs are common in semiconductor devices. In a Metal–Oxide–Semiconductor Field–Effect–Transistor (MOSFET) the applied gate voltage creates an inversion layer of charge carriers, right below the gate oxide. Electrons (or holes) are confined at this interface and can only move in the lateral plane. In a High Electron Mobility Transistor (HEMT), a 2DEG is created as a result of band bending at the junction between AlGaAs and GaAs [12].

Since the discovery of a 2DEG at the LAO/STO interface, it as been the subject of extensive research. At first, it is a striking feature that mobile charge carriers occur at the interface since both of the materials themselves are insulators. Additional publications reporting on properties like superconductivity and magnetoresistivity have helped spark interest in this interface [7, 8].

However, the origin of the charge carriers at the interface is still a disputed topic [13]. A In their original paper, Ohtomo and Hwang proposed the electronic reconstruction model to explain the phenomenon [6]. This model has since been widely cited, and is also used for most theoretical descriptions of the interface. However, in later years several groups have published results that questions the model and asks for a more complex description of the interface [2, 14, 15].

2.1 Materials

2.1.1 Perovskite oxides

Both STO and LAO belong to the perovskite oxide family of materials, and they are also sometimes referred to as *complex oxides* or *transition metal oxides*. The term transition metal refers to an element whose atom has an incomplete d sub–shell, or which can give rise to cations with an incomplete d sub–shell [16]. A complex oxide is an inorganic solid with multiple metal cations and oxygen anions [2]. The term perovskite refers to a specific crystal structure of materials with the chemical formula ABO_3. In this formula A and B are two cations of different size and O is the oxygen atom and the A atom is always larger than the B atom. A perovskite cubic unit cell is shown in Figure 1(a). In this unit cell the B atoms sit at the corners, the A atom is in the body centre position and O atoms are found at every edge. At room temperature STO has this cubic structure depicted in the figure while LAO is rhombohedrally distorted, i.e the unit cell is stretched along the body diagonal.

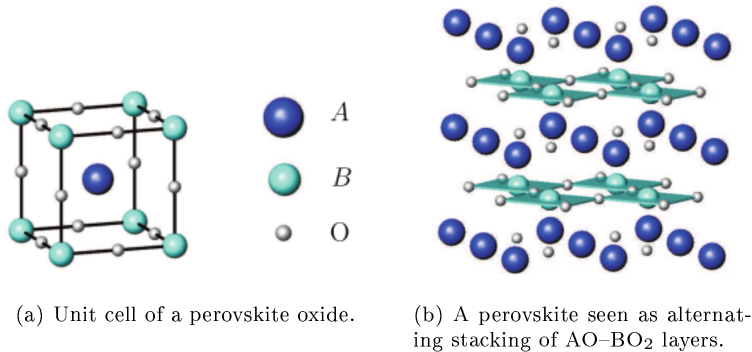

(a) Unit cell of a perovskite oxide.

(b) A perovskite seen as alternating stacking of AO–BO_2 layers.

Figure 1: The perovskite oxide crystal structure, ABO_3, from [17]

2.1.2 The LAO/STO interface

Another way of looking at the perovskite structure is as a stacking of alternating layers of AO and BO_2 along the z direction. This view is illustrated in Figure 1(b). When thinking about the materials in this way, LAO is viewed as a stacking of alternating layers of LAO and AlO_2. In the same way STO is seen as alternating SrO and TiO_2 layers [14].

The most common way to prepare the interface is to grow a thin film of LAO on top of an STO substrate by PLD (more on growth in Section 2.4) [18]. The substrate is treated to have a single termination, meaning the top layer is either SrO or TiO_2 and this is consistent across the whole surface.

The consequence is that two different interfaces are possible. Either a AlO_2/SrO (called p–type) or a LaO/TiO_2 (n–type) interface will define the transition from one material to the other. Both types of interfaces can be manufactured. However, one of the striking discoveries is that only the n–type is conductive while the p–type remains insulating [6]. The fact that one atom layer can have such a profound effect on the electrical properties is remarkable.

2.1.3 Step–and-terrace surface

The STO substrates are treated to have a single termination. Nevertheless, the surface is not atomically flat. When the substrates are cut, there is always a slight misalignment; the cutting angle along the surface is not perfectly aligned with the crystal plane. The angle between the crystal plane and cutting angle

is called the miss–cut angle or vicinal angle.

As a result, the substrates have a step–and–terrace topography on the surface (Figure 2). The step heights for a single terminated substrate are always 1 unit cell (u.c.) thick (3.9Å), and the terrace width depends on the vicinal angle. A larger angle means smaller terraces. The vicinal angle for the example in Figure 2 is 0.08°.

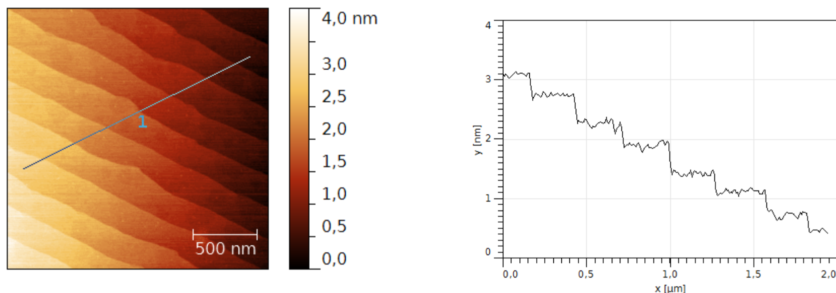

(a) The step–and–terrace topography is clearly visible in AFM images

(b) The profile shows that every step height is 1 u.c.

Figure 2: AFM image and height profile of a TiO_2 terminated STO substrate.

2.2 Interface properties

There are 4 major observations which have been reproduced by numerous groups: (1) the interface is only conducting if the substrate is TiO_2 terminated prior to growth i.e. the n–type interface (LaO/TiO_2) is conducting, while the p–type (AlO_2/SrO) is insulating. (2) There is a critical thickness of the film before the interface becomes conducting. For a single film of LAO on top of STO this is 4 u.c. (3) Above the critical thickness the conductivity is independent of film thickness. (4) The conductivity is strongly dependent on deposition conditions; in particular the oxygen pressure during growth [1, 2].

2.3 Modelling the interface

2.3.1 Electronic reconstruction

When Ohtomo and Hwang first discovered the conductive interface between LAO/STO they also proposed a model to explain the effect, dubbed "electronic

reconstruction".

In STO both layers $Sr^{2+}O^{2-}$ and $Ti^{4+}O_2^{4-}$, are charge-neutral, but in LAO the story is different: $La^{3+}O^{2-}$ has a net positive charge while $Al^{3+}O_2^{4-}$ is negative. Figure 3(a) illustrates this charge distribution and shows the induced electric field along the z axis. The potential in the film as a result of this field increases linearly with increasing LAO thickness. But this diverging potential is not energetically feasible. It will increase towards infinity as the film gets thicker. This problem is often called the *polar catastrophe* in literature. As a consequence of this, the electric field needs to be screened, i.e some charge has to move. The electronic reconstruction model is a relatively simple one. In short: electrons move from the LAO film to the interface until the potential is screened. If 0.5 electrons per unit cell moves to the interface, this charge is enough to screen the potential. In Figure 3(b) this case is shown graphically. Instead of a steadily increasing potential along the z-axis, the electric field will now oscillate around zero[1] and produce a finite potential. The theory also predicts that this will happen at a certain thickness — when the energy cost of moving the electrons is smaller than increasing the potential. Calculations of the critical thickness using this model coincides with the experimentally observed thickness of 4 u.c.

The case in Figure 3(a) and 3(b) where the interface is LaO/TiO_2 is called n–type because *electrons* will move to the interface and become the majority charge carriers. The other possible interface (AlO_2/SrO) would need holes at the interface and is accordingly dubbed p–type

The transfer of electrons to the interface is feasible because the Ti atom is multivalent, it can take up another electron in its outermost shell. On the other hand no atom that can take up another hole is present. The theory thus predicts that a n–type interface will be conducting and the charge carriers will move in the valence band of the Ti atoms at the interface. On the other hand a p–type interface will not be able to compensate by electronic reconstruction, because no atom at the interface can take up another hole. This fits well with the experiments which show that the n–type interfaces are conducting and p–type interfaces are insulating [6].

2.3.2 Criticism to electronic reconstruction

Several authors have published reports which call into question using only the electronic reconstruction model to describe the interface. They argue that the

[1] as a function of distance in the film, not time

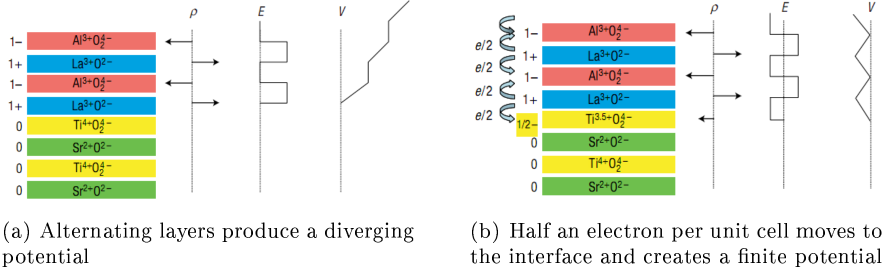

(a) Alternating layers produce a diverging potential

(b) Half an electron per unit cell moves to the interface and creates a finite potential

Figure 3: The alternating polar layers of LAO grown on neutral STO produces an electric potential that diverges with thickness. Compensation is done by moving electrons to the LAO/STO interface. From [14]

processes which occur at the interface are more complex. Effects such as oxygen vacancies, cation intermixing and doping have to be considered to give an accurate description of the interface.

In the electronic reconstruction model the interface is assumed to be abrupt, meaning there is a point along the z–axis where the material goes from strictly LAO to strictly STO. No Sr or Ti is assumed at the LAO side of the interface and vice versa, no La or Al is assumed at the STO side. Only electrons move in response to the potential buildup in the film [14].

In contrast, Willmott *et. al.* used surface x–ray diffraction (SXRD) to probe the elements at different depths around the interface, and found that there *is* significant intermixing [15]. A plot taken from this report is shown in Figure 4. In the plot, stochiometry is plotted as a function of position along the z–axis. Cation intermixing exists on both sides of the interface. Moreover, La and Sr intermix deeper in the substrate than does Al and Ti.

Other reports have reached similar conclusions. Qiao *et. al.* demonstrated, with the use of rutherford backscattering and secondary–ion–mass spectrometries, that both La and Sr diffused across the interface [18]. Chambers *et. al.* used several analytical methods to analyze the abruptness of the interface and found evidence of a strong tendency towards intermixing [2]. They show traces of La several hundred Angstroms below the interface. They also performed theoretical calculations indicating that a rough interface is more thermodynamically stable than an abrupt one. Nakagawa *et. al.* found that the p–type interface is more abrupt (less intermixing) than the n–type [14].

Segal *et. al.* have measured the built–in electrical field in the LAO film with

X-Ray Photoemission Spectroscopy (XPS) [19]. This field should, according to the electronic reconstruction model, be 1.15 ± 0.06V/uc. In experiments however, the field is not observed.

The electronic reconstruction model also fails to explain the insulating properties of samples grown at high oxygen pressure. Models which introduce oxygen vacancies and cation diffusion can predict this by taking into account that fewer vacancies are created at high pressure [20].

2.3.3 La doping

STO is by itself an insulating material with a band gap of 3.2eV. However by doping the material with Nb or La, the material can obtain semiconducting or metallic transport properties [21]. La acts as an n–type dopant in STO when the ions substitute the Sr positions and becomes electrically active. Willmott *et. al.* have noted that $La_{1-x}Sr_xTiO_3$ is conducting for x between 0.05 and 0.95 [15].

However, also Al diffuses into the substrate and contrary to La, the Al ion act as an *acceptor* in STO. Since the interface is n–type this suggests that, if La doping is the main cause for the observed conductivity, the composition is $La_{1-x}Sr_xAl_{1-y}Ti_yO_3$ with $x < y$.

Chambers *et. al.* note that the measured La areal density in the top 1-2nm of STO is enough to account for the observed sheet carrier concentration if some of the indiffused atoms becomes electrically active. The measured La areal density is $\sim$2–4$\times10^{14}$cm^{-2} which is about 20 times larger than the reported sheet carrier concentration of $\sim$1–2$\times10^{-13}$cm^{-2} [2].

2.3.4 Oxygen vacancies

Oxygen vacancies are common defects in STO. When removed from the lattice, each oxygen is expected to donate one or two electrons to the conduction band [22]. Experimentally it is found that each vacancy donates a little less than 1 electron. Furthermore, it is found that the oxygen vacancies are not evenly distributed in the crystal, but tend to form clusters [23].

To induce oxygen vacancies in STO, a substrate is heated in a low oxygen pressure. Annealing at 800°C at 10^{-6} mbar makes the substrate highly conductive [10].

Kalbukhov *et. al.* have used cathode luminescence to detect oxygen vacancies for LAO/STO interfaces grown at different oxygen pressures. Their results show both increased conductivity and more oxygen vacancies at low pressure

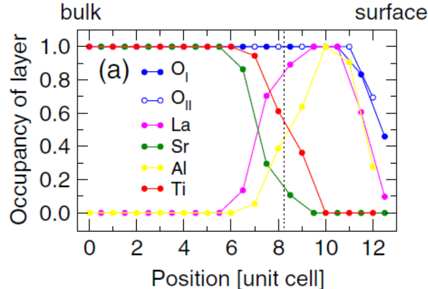

Figure 4: Layer compositions as determined by SXRD. The plot shows that there are significant cation intermixing and that La/Sr intermix deeper in the STO than does Al/Ti. From [15]

(10^{-6} mbar), compared to high pressure samples. However, oxygen vacancies are also identified in high pressure samples (10^{-4} mbar). Moreover, after re–entering oxygen in the low pressure samples, both the conductivity and oxygen vacancy concentration are similar to the high pressure samples. Their conclusion is that most of the observed conductivity, also in high pressure samples, stem from oxygen vacancies and only a small contribution, if any comes from the polar catastrophe [10].

2.4 Introduction to thin film growth with PLD

PLD is a Physical Vapor Deposition (PVD) process which have become popular because of its relatively cheap and simple implementation [9] and its ability to create high quality oxide interfaces [5]. A simple schematic of the setup is depicted in Figure 5.[2]

A substrate and target (the material which is going to be deposited) is placed in a growth chamber facing each other. A pulsed laser is directed onto the target. When a laser pulse is absorbed by the target, species (atoms, ions, molecules etc.) are ejected from the surface and move towards the substrate. Right after being ejected, the species absorb some of the laser energy themselves, creating a plasma plume.

When growing complex inorganics (such as LAO and STO) with PLD, the

[2]This figure depicts an off–axis configuration, see Section 3.2.1. Normally the substrate is placed directly across from the target (i.e $\theta = 0°$).

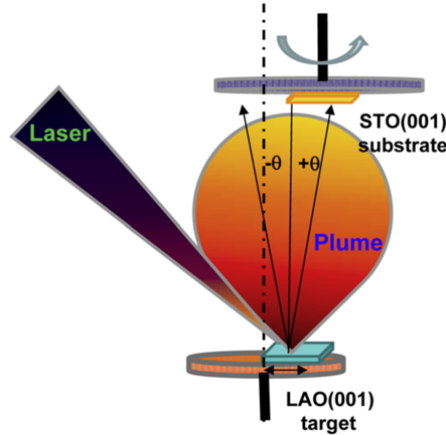

Figure 5: Schematic diagram of an PLD setup. From [24]

ejected species needs to be mainly atomic, diatomic or other low–mass particles. To achieve this, the energy of the laser pulse needs to be strongly absorbed in a small volume of the target. As a result, a small–wavelength (UV) laser and a short pulse (nanoseconds) is required [9].

In the growth chamber a background gas is present, which affects the deposition in two ways. The gas often reacts chemically and is used to create the correct stochiometry of the thin film. For example, an oxide grown under too low oxygen pressure will result in oxygen deficiencies in the film. The other use of the background gas is that it reduces the kinetic energy of the ejected species. Since often a high pulse energy is needed to achieve ablation, the ejected species themselves will have a high energy. Atoms and ions with too high energy will be able to penetrate into the substrate and cause defects in the material and damage the surface. When a background gas is present the species will collide with gas molecules and lose some of their kinetic energy before reaching the substrate [9].

When the species reach the substrate, they will be adsorbed. The deposited species will nucleate and grow epitaxially on the substrate. The substrate often has to be heated to a certain temperature for the nucleation to occur.

One problem with PLD is that the material flux is both directional and has a small radius. If the substrate is too large, both non–uniform thickness and also variations in the stochiometry will occur [9].

2.5 Summary

A 2DEG has been demonstrated at the interface between the two band insulators LAO and STO. A critical thickness of the thin film defines the transition from insulating to conducting; for a single LAO film on bulk STO this thickness is 4 u.c. Two types of interfaces are possible depending on the substrate termination and are dubbed n–type and p–type. In experiments only n–type interfaces are conducting.

Several models have been proposed to explain the origin of the charge carriers. The most widely used is called electronic reconstruction and generally assumes a perfectly abrupt interface. However, several publications have found evidence that the interfaces is *not* abrupt and thus the tendency have shifted towards explaining the conductivity in more complex terms and include effects such as cation intermixing, La doping and oxygen vacancies.

The interface is most commonly prepared with PLD. The method is relatively cheap and simple in its implementation, but has the ability to create high quality interfaces with atomic layer precision.

3 Experimental

3.1 The sample creation process

To create a sample, an STO(001) crystal is used as a substrate. On top of the substrate, a thin LAO film is grown by PLD. After this, metal contacts to the interface are made. The metal is deposited with an electron–beam evaporator, and either a wire bonder or a scalpel is used to make sure the metal is in contact with the interface. [3]

3.1.1 Preparing the substrate for PLD growth

Only n–type interfaces will be grown in this project, and the substrates are already TiO_2 terminated from the manufacturer. They are ordered from Shinkosha Co. and come as single crystals with (001) lattice orientation. When received, the substrates have $0.5 \times 15 \times 15$ mm dimensions. They are first cut into 5×5 mm pieces with a diamond saw and then cleaned. In the cleaning process they are immersed first in acetone, then ethanol. Both cleaning steps are performed in an ultrasonic bath for 5 minutes. Afterwards they are blow dried with a nitrogen gun to remove any residue of the cleaning agents.

The substrates are then annealed in atmospheric pressure O_2 for 2 hours at 950°C . After annealing the substrates have the expected step–and–terrace surface which is verified by Atomic Force Microscopy (AFM) images. Conditions include that the step edges are straight (no meandering) and that the step heights are 1 u.c. (3.9Å).

3.1.2 Thin film growth with PLD

Before growth the substrate is again rinsed with acetone and ethanol in an ultrasonic bath. The substrate is then mounted on a sample holder with silver paste glue. The glue is cured by heating on a hotplate at 150°C for 1h. After this, the substrate is inserted into the growth chamber via a loadlock.

The chamber is pumped to the desired deposition pressure, which is in the range 10^{-2} to 10^{-4} mbar. The substrate itself is heated to $500 - 800$°C at a rate of 15°C/min. An optical pyrometer is used to measure the substrate surface temperature.

[3] Ideally, we would like to use ion etching to create small holes in the LAO film followed by metallization. However no ion etcher is available at NTNU NanoLab and thus we resort to the described methods.

The laser is a KrF eximer laser with $\lambda = 248$nm. The most homogeneous part of the laser beam is selected by passing the beam through a rectangular metal mask. The beam is focused in such a way that the spot size (the area on the target which is hit by the laser pulse) is a few square millimeters[4]. The *laser fluence* [J/cm^2] is the amount of energy (divided by the spot size) in the laser pulse when it reaches the target:

$$\phi = \frac{E}{A} \tag{1}$$

where E is the total energy of the laser pulse at impact, and A is the spot size. The laser power is controlled by adjusting the input voltage. Thus, laser fluence is a function of the voltage, mask size and focusing of the laser beam.

The growth is performed with the laser pulse frequency at 1Hz. Film thickness is controlled by monitoring Reflection High Energy Electron Diffraction (RHEED) intensity oscillations of the specular spot (see Section 3.2.5). When the desired number of unit cells has been grown (= number of RHEED intensity peaks), the laser is shut off and deposition stops.

After growth the sample is cooled down to room temperature. This takes about 2 hours and the oxygen pressure during cooling is kept at 100mbar.

Various parameters will be adjusted when growing samples. This is detailed in Section 3.2.1.

3.1.3 Creating electrical contact to the interface

Two different methods are used to make electrical contact to the interface. One makes use of a scalpel, the other a wire bonder. In earlier work the scalpel method have been used with success, but the wire bonder method was only briefly used, due to downtime of the equipment [11]. As the wire bonder method is expected to produce better contacts, an effort to optimize this process is performed in this project.

Wire bonder method A goal for this project is to develop a contact creation process which creates the same contact pattern on every sample. For this, a shadow mask was designed. Figure 7(a) depicts the shadow mask pattern. The shadow mask is made from a 0.1 mm thick steel plate with holes drilled as indicated in the figure. During metal deposition, the shadow mask is placed in front of the sample. The mask is kept in place by a mask holder, shown in

[4]The spot size is 2.52mm^2 for the majority of the samples. However, during the laser fluence series this was varied, see Section 3.2.1 and 4.2.

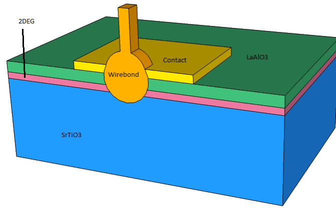

(a) Illustration of how the wire bond method will make contact to the interface

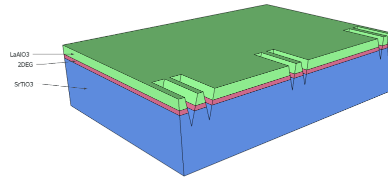

(b) Illustration of a sample after scratches have been made with a scalpel. Afterwards metal will be deposited at the scratched areas and come in contact with the interface at the sidewalls of the trenches.

Figure 6: Illustration of the contact methods

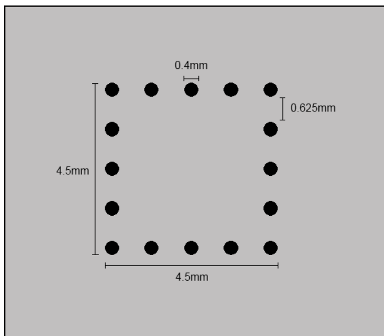

(a) The shadow mask layout. The black dots represent holes drilled through the metal plate.

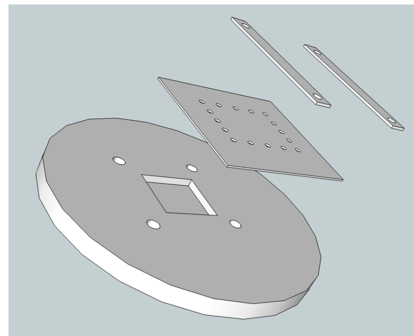

(b) Illustration of the mask holder. The shadow mask is kept in place by two steel strips which are attached to the holder by screws. Dimensions are not to scale.

Figure 7: Shadow mask and holder

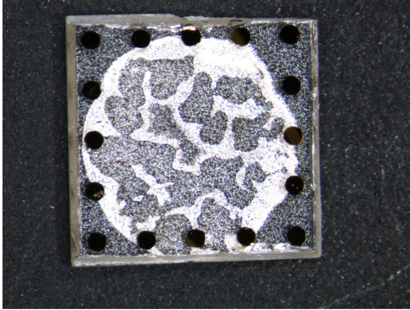

(a) Sample after metal deposition through the shadow mask

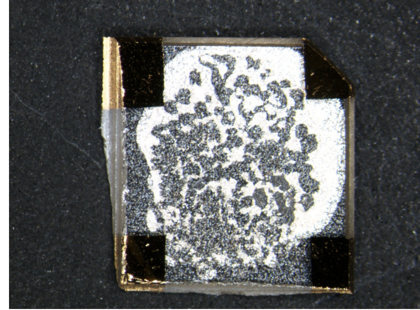

(b) Sample after metal deposition with scotch tape mask

Figure 8: Typical images of samples after metal deposition

Figure 7(b). This holder is 3 mm thick and made from aluminum. The holder is shaped as a disk with a 150 mm diameter to fit the sample holder in the electron–beam evaporator. In the center of the disk a 0.7 mm deep grove is made to hold the sample. The mask is kept in place above the sample with two strips of steel which are screwed tight at the four corners of the grove. The contact pattern is 4.5×4.5mm. It is made somewhat smaller than the 5×5 mm samples, because there are always some variations in sample size.

Metal is deposited with the shadow mask in front of the sample. Even though metal has been deposited at the surface of the sample, there is still no connection to the interface. The metal has to penetrate through the thin film. One way to make this happen is to use a wire bonder. The wire bonder used here is a TPT HB05. When a bond is made with the wire bonder at one of the metal pads, ultrasonic energy (vibration) and pressure will be applied to the pad. If the energy is high enough to penetrate through the film, a direct electrical contact will be made to the interface, see Figure 6(a). The assumption that the wire bond will penetrate through the film is reasonable because of how thin the films are (< 20nm).

The wire bonder has several parameters that can be adjusted by the operator. The parameters are ultrasonic energy, the time which the energy is applied, temperature and downward force. The parameters have to be calibrated to obtain good bonds. A test sample which is covered with metal (no contact pattern) is used to calibrate the parameters. The test sample is a single crystal STO or LAO substrate, and the metal composition is the same as the real sample

we want to bond.

Scalpel method The other method available for making contacts is the scalpel method employed in [11]. In this method scratches on the surface are made in separated regions (corners of the sample). These scratches will penetrate through the LAO film and into the STO substrate, leaving the interface exposed at the sidewalls of the trenches (Figure 6(b)). The sample is then masked with thin strips of scotch tape: the area between the scratched regions are covered with tape, leaving the scratched regions exposed. Metal will be deposited in, and around the trenches. After deposition the scotch tape is removed. This will act as a lift–off process – metal will only be left in the non–masked regions. Since the metal will cover the sidewalls of the trenches it will be in direct contact with the conductive interface.

Metal deposition by electron–beam evaporation In both methods described above, the metal is deposited by electron–beam evaporation. In this process metal is heated up by bombardment of a electron–beam. As the metal becomes warmer it starts to evaporate. The process is done at low pressure, the pressure in the deposition chamber is kept at $\sim 10^{-7}$ mbar.

The metal target is positioned at the bottom of the chamber and the sample is placed upside–down near the top. The sample is masked by either scotch tape or the shadow mask, depending on the process. If the sample is masked by scotch tape it will have 4 contacts at the corners. The shadow mask will leave 16 circular pads along the edges of the sample. Pictures of samples masked with both methods are shown in Figure 8.

The evaporator has a target carousel which allow for multiple depositions of different metals. Unless otherwise noted, a 10nm Ti adhesion layer followed by 100nm of Au is deposited on the samples.

3.2 Characterization

3.2.1 Tuning growth parameters

There are several parameters in a PLD system that influences the growth and quality of the film. This parameter space will be explored in order to improve the interface quality and the samples will be compared in terms of their sheet resistance. The aim is to come close to what is reported in literature, $\sim 10^4\Omega/\square$ at room temperature.

In earlier work the sheet resistance of several pre–grown samples have been measured [11]. Most of the previously studied samples had sheet resistances way above $10^5\Omega/\square$. However, these where thick films, > 30 u.c. It has been shown by Thiel that LAO films grown on STO will start to relax around 25 u.c. and that films thicker than this tend to be insulating [17]. For this reason, thin films have been grown for this report. The majority of samples have an LAO thickness of 10 u.c.

The various PLD parameters which can be controlled are:

- Oxygen pressure
- Laser fluence
- Substrate–target distance
- Off–axis angle
- Substrate temperature

Series will be grown where each of these parameters are varied while the others are kept constant. Tables 2, 3, 4, 5 and 6 list the growth parameters for each series.

Oxygen pressure In literature, the oxygen pressure is the most critical process parameter reported. It is known to have a large impact on the sheet resistance. A low oxygen pressure (10^{-6} mbar) will introduce oxygen vacancies in the STO. A high oxygen pressure (> 10^{-2} mbar) have been shown to induce island growth instead of the desired layer–by–layer growth mode [1].

In this project samples will be grown with oxygen pressures of 10^{-2}, 10^{-3} and 10^{-4} mbar which is the lowest operating pressure of our PLD system.

Table 2: Oxygen pressure series. All films are 10 u.c. thick, spot size is 2.5 mm^2 and substrate–target distance is 45 mm.

Sample	Pressure	Temp.	Contacts	Fluence
p10217	10^{-2} mbar	568°C	scalpel	1.79 J/cm^2
p10301	10^{-3} mbar	595°C	scalpel	1.79 J/cm^2
p10302	10^{-4} mbar	634°C	scalpel	1.79 J/cm^2

Table 3: Laser fluence series. All films are 10 u.c. thick, grown at 10^{-3} mbar and substrate–target distance is 45 mm.

Sample	Fluence	Spot size	Temp.	Contacts
p10402	1.43 J/cm^2	2.5 mm^2	670°C	wire bond
p10403	1.07 J/cm^2	2.5 mm^2	654°C	wire bond
p10516	1.06 J/cm^2	1.7 mm^2	687°C	scalpel
p10602	2.28 J/cm^2	2.3 mm^2	680°C	scalpel
p10606	0.70 J/cm^2	5.3 mm^2	628°C	scalpel

Table 4: Substrate–target distance series. All films are 10 u.c. thick, grown at 10^{-3} mbar, spot size is 2.5 mm^2 and substrate–target distance is 45 mm.

Sample	Dist.	Temp.	Contacts	Fluence
p10402	45 mm	670°C	wire bond	1.43 J/cm^2
p10514	50 mm	687°C	scalpel	1.43 J/cm^2
p10515	55 mm	678°C	scalpel	1.43 J/cm^2

Table 5: Off–axis angle series. All films are 10 u.c. thick and grown at 10^{-3} mbar, spot size is 2.5 mm^2 and substrate–target distance is 45 mm.

Sample	Angle	Temp.	Contacts	Fluence
p10402	0°	670°C	wire bond	1.43 J/cm^2
p10509	6.5°	677°C	scalpel	1.43 J/cm^2
p10511	16.6°	677°C	scalpel	1.43 J/cm^2
p10512	10.8°	661°C	scalpel	1.43 J/cm^2
p10601	-9.8°	683°C	scalpel	1.18 J/cm^2

Table 6: Substrate temperature series. All films are grown at 10^{-2} mbar, fluence is 1.79 J/cm^2 and spot size is 2.5 mm^2 and substrate–target distance is 45 mm.

Sample	Temp.	Thickness	Contacts
p10109	586°C	10 u.c.	wire bond
p10201	579°C	8 u.c.	wire bond
p10217	568°C	10 u.c.	scalpel
p10218	614°C	15 u.c.	scalpel

Laser fluence In literature, laser fluences are usually between 1 and 2 J/cm^2 [1]. However, lower values have also been reported. For instance Xie *et. al.* used a laser fluence of 0.67J/cm° [25].

There are two ways to adjust the laser fluence. The intensity of the laser is controlled manually by adjusting the input voltage. The other option is to change the mask area. Increasing the mask area lets more of the beam through, thus more energy. However, this also increases spot area, which in turn lowers the laser fluence, see Eq (1).

The laser fluence is adjusted in both ways. Table 3 lists the fluences and also the spot sizes for each of the samples in this series. The spot size is found by measuring the visible area left by the laser pulse on the target crystal. The energy of a laser pulse is measured by a detector placed in front of the growth chamber where the laser pulse enters. A 10% loss of the chamber window is taken into account.

Substrate–target distance The distance between substrate and target will also affect the kinetic energy of the ablated atoms when they hit the substrate. As the ablated species move from the target to the substrate, they will frequently collide with the oxygen molecules present in the chamber. Each collision reduces the kinetic energy of of the interacting atom. A longer distance means more collisions and thus a lower kinetic energy of the species when they hit the substrate.

The substrate–target distance is altered by moving the substrate stage away and towards the target.

Off–axis angle The angle θ in Figure 5 is called the off–axis angle. It is a measure of the substrate displacement relative to the target (and thus the material flux).

PLD is generally thought of as a stoichiometric transfer. After growth, the film is assumed to have the same stoichiometry as the target. However, this is not always the case. Qiao *et. al.* have shown that the La:Al cation ratio can be varied by *off–axis* deposition of the LAO film [18].

The off–axis angle will be adjusted in the same plane as the incoming laser beam. A positive θ means away from the direction the laser beam enters. The angle is adjusted by moving the substrate stage. Referring to Figure 5, the substrate stage is moved to the left and right.

Substrate temperature Substrate temperature controlled by adjusting the current and voltage through a platinum coil which is located behind the substrate. The current voltage is adjusted by a regulater conntected in a feedback loop with a temperature sensor. The temperature sensor is located right by one side of the substrate. However, this sensor is not accurate enough and thus an optical pyrometer is used to measure the substrate temperature. The temperature is measured immediately before and after growth, and the average of these two measurements is taken as the deposition temperature.

3.2.2 Examining surface topography with AFM

AFM is a technique to measure the topography of a surface with very high precision. The technique uses a cantilever with a sharp tip which is brought close to the surface. The force between the sample and the tip is measured and the tip is scanned across the surface to make a topographical image of the surface.

There are several modes of AFM. In *contact mode* the tip is is contact with the surface. The tip is scanned across the surface and when it encounters obstacles it will be deflected. The cantilever is made of a piezoelectric material which induces a voltage in response to the deflection. This voltage is then used as a measure of the topography.

The mode used in this project is called *tapping mode.* In tapping mode the cantilever is not in contact with the surface but kept oscillating close to its resonance frequency. The distance between the surface and the cantilever is such that the top touches the surface only at the lowest point of deflection. If the tip comes closer to the surface (it moves towards an uphill slope) the attractive forces causes the amplitude to decrease. By using a feedback loop

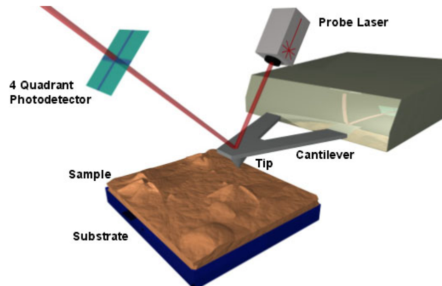

Figure 9: Illustration of an AFM setup, from [26]

the tip is accordingly lifted until the amplitude reaches its setpoint again. The amplitude is in this way kept constant by the feedback loop. The height which the tip is raised and lowered by, is used to produce the image of the surface.

A laser and photodetector is used to measure the amplitude of the cantilever. The laser is pointed at the cantilever and reflected off to a photodetector, see Figure 9. As the cantilever oscillates, the laser beam will scan along a line on the detector [27].

3.2.3 Sheet resistance measurements

The sheet resistance, $R_{\square}$, is measured with the van der Pauw method. A four–probe measurement station connected to a computer is used to record the data. The measurement setup is described in [11].

When calculating the sheet resistance, several measurements are done. In each measurement current is fed through one side of the sample (the current probes are placed at two corners sharing the same side) and voltage is recorded at the other side. There are four possible such combinations of voltage and current. For each permutation two measurements are done, one for each current direction, giving a total of 8 measurements.

The average resistance measured in the x direction (when current is passed in the vertical direction in Figure 10) is called R_x. The resistance measured in the y direction is similarly called R_y and the van der Pauw equation[28] becomes [11]:

$$e^{-\pi R_x/R_{\square}} + e^{-\pi R_y/R_{\square}} = 1 \tag{2}$$

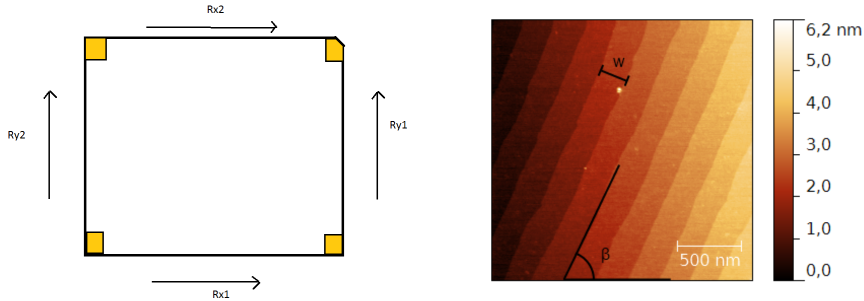

(a) Schematic of a sample indicating notations used when discussing direction dependent resistance.

(b) AFM image with terrace width, w and step angle, β indicated

Figure 10: Comparison between resistance measurements and AFM images. R_{x1} is the case where *current* is passed through the bottom two contacts in (a) and voltage is measured across top two. The other values are defined in the same way.

Equation (2) is evaluated numerically with Matlab. The script file can be found in Appendix A.

Earlier work has shown that the sheet resistance is direction dependent [11]. When measuring the sheet resistance, the resistance measured in the x direction was significantly different from the measurements in the y direction.

$$R_x \neq R_y \tag{3}$$

To look for a correlation between the direction dependent resistance and the step–and–terrace topography, the sheet resistance measurements will be compared with AFM pictures. The AFM and sheet resistance measurements are aligned so the results can be directly compared. In Figure 10(b) an AFM image is shown with the step angle and terrace width indicated. The step angle is defined as the *smallest* angle between the x–axis and a step edge. This is because of symmetry: current is passed in both directions and along both edges of the sample. Thus the step angles used when comparing samples are always less than 90°.

Note that

$$R_x = \frac{R_{x1} + R_{x2}}{2} \tag{4}$$

and R_y is defined in the same manner.

3.2.4 Contact characterization

The contact resistance (the resistance between the 2DEG and the metal contact), is an easily quantifiable characteristic of a contact. This parameter is commonly measured with Transmission Line Measurements (TLMs). At least 4 contacts along the edge is required to measure the contact resistance of the corner contacts [11]. The contact pattern from the shadow mask is made to allow TLMs with 5 contacts along each edge.

TLMs on scalpel prepared samples have been tried earlier. However, the results were unreliable and did not produce good estimates for the contacts resistance [11]. For this reason no TLMs will be performed on scalpel prepared samples. The contact pattern for these samples consists of only 4 corner contacts, enough to do van der Pauw measurements.

Another method will be used to evaluate the scalpel prepared contacts. The method makes use of the fact that when the sheet resistance is measured, several redundant measurements are done. In principle only two measurements are needed to calculate the sheet resistance [28]. Since 8 measurements are done, there are several redundant measurements which can be examined. In principle the contact resistance should not affect a van der Pauw sheet resistance measurement [28]. However, if contact quality affects the measurements, statistical deviations in the individual measurements are expected.

One such test is if the measured resistance changes when current direction is switched. To evaluate this, a parameter γ is defined as the difference between positive and negative measurement, relative to the average of the two:

$$\gamma = \frac{abs(R^+ - R^-)}{(R^+ + R^-)/2} \times 100\% \tag{5}$$

where R^+ and R^- are the outcomes of a resistance measurement when current is passed in the positive and negative direction, respectively. The reasoning behind making the difference *relative to the average* is to ease the comparison between samples. The samples themselves may have large differences in the absolute value of the sheet resistance. With Eq (5) the values are transformed into percentages, which can easily be compared.

It was stated above that the sheet resistance is anisotropic, see Eq (3). However, the resistance measurements taken on parallel sides of a sample should yield the same results, i.e. $R_{x1} = R_{x2}$. This provides another method to evaluate

the influence of the contacts. A new metric, δ, is defined in the same manner as above:

$$\delta = \frac{abs(R_{x1} - R_{x2})}{(R_{x1} + R_{x2})/2} \times 100\% \tag{6}$$

The parameter δ is a measure on how well the measurements taken on opposite sides agree. Thus, if the direction dependent resistance is an intrinsic effect of the sheet resistance and the influence of contacts are low, δ should be small. The measurements in the y direction are included by substituting R_{y1} for R_{x1} and R_{y2} for R_{x2} in Eq (6).

3.2.5 Growth monitoring with RHEED

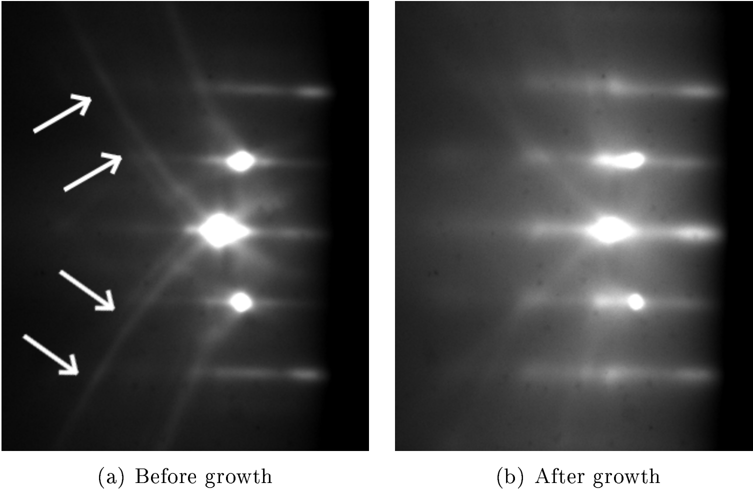

(a) Before growth (b) After growth

Figure 11: RHEED images taken before and after growth of a 10 u.c. LAO film

During deposition *in situ* RHEED is used to check the surface quality and measure the film thickness. An electron beam incident on the sample surface is reflected and diffracted by the surface atoms. A phosphor screen acting as a detector collects the reflected electrons. When the electrons hit the screen, it will light up at the point of impact. A CCD camera is placed behind the screen and sends the live image to a computer.

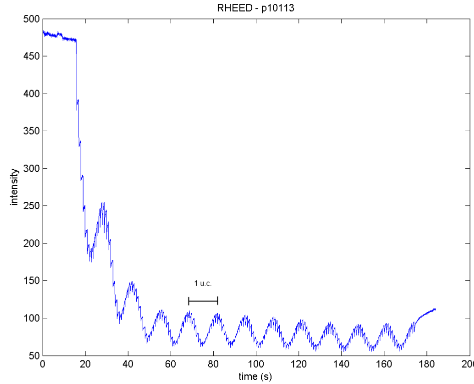

Figure 12: Measured RHEED intensity oscillations during the growth of a 12 u.c. thick LAO film.

The electrons form a diffraction pattern on the detector. The electron beam has a small incident angle relative to the sample surface (typically 0.1° - 5°) [29]. Moreover, the penetration depth is only a few atom layers, thus the electrons are reflected and diffracted only by the surface atoms. Since the electrons only interact with the atoms at the surface, this pattern give insight into the surface structure of the sample. The coherence length, meaning the distance between reflected electrons which can interfere with each other is in the order of several hundred nanometers. Thus the diffraction pattern represents a fairly large part of the surface area.

A RHEED image of an STO surface diffraction pattern is shown in Figure 11(a). The diffraction spots lie on concentric circles. The brightest spot is the specular spot, and the two adjacent ones correspond to (01) and $(0\bar{1})$ reflections. The kikuchi lines indicated by arrows originate from diffuse scattering and indicates a flat and crystalline surface. On the other hand, streaks in the pattern, as for the LAO film in Figure 11(b), is a sign of a rougher surface [29].

During growth the intensity of the specular spot is measured and plotted. When the first atoms hit the substrate, they will deposit randomly on the surface. As such, the surface looks more 'chaotic' and accordingly the RHEED intensity drops. However, when a whole unit cell has been deposited the surface again looks well ordered and the intensity is high again. Accordingly, the intensity will oscillate where each period of the oscillations corresponds to one

grown unit cell. An example of a RHEED intensity oscillation plot is given in Figure 12. This is used to determine the thickness of the film. During growth this intensity is monitored and deposition is stopped after the desired number of unit cells is reached.

3.2.6 Crystal quality verification with XRD

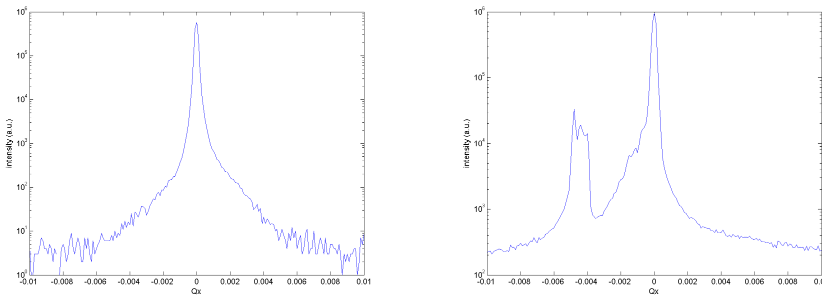

(a) Only one peak, indicating a single domain (b) Multiple peaks, indicating more than one domain

Figure 13: Examples of XRD rocking curve plots

The substrates are also analyzed with X–Ray Diffraction (XRD) to verify the crystal quality. The substrate is aligned so the Bragg condition is fulfilled for two subsequent monolayers along the vertical direction. A rocking curve scan (θ–scan) is then performed. If the substrate is completely monocrystalline only one peak will show up on the detector. However, if multiple domains exists (which are rotated relative to each other) multiple peaks will occur, at different angles. The plot in Figure 13(a) is an example of a good substrate and is later used for film growth. The result in Figure 13(b) is from a substrate with multiple crystal domains. Substrates like this are discarded.

3.3 Summary

Samples are made by growing a thin LAO film on a TiO_2 terminated, STO(001) substrate. Various PLD parameters will be optimized in order to create a high quality n–type interface. Metal contacts to the interface are made by one of two methods. The first method uses a shadow mask when depositing metal,

and then applying wire bonds on the metal pads to reach the interface. The second method creates contact trenches with a scalpel and then deposits metal with scotch tape as a mask.

Characterization is done by comparing sheet resistances, which is measured with the van der Pauw method. AFM images are used to look for correlation between direction dependent sheet resistance and the step–and–terrace topography.

The contacts themselves will be analyzed in terms of the creation process and impact on sheet resistance measurements.

4 Results

4.1 Contacts

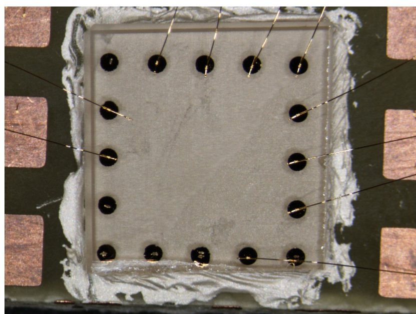

(a) Sample after a failed bonding attempt. 5 contacts failed to bond and on these contacts the metal peeled off during bonding attempts.

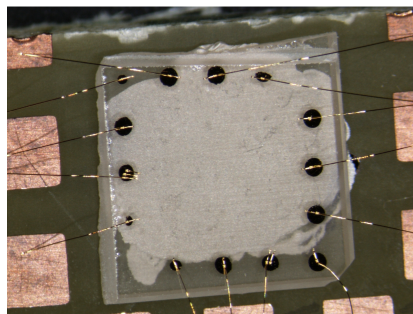

(b) A sample where some metal pads have been removed in an ultrasonic bath prior to bonding. Bonding was successful on all remaining pads.

Figure 14: Samples after bonding

Wire bonder method When performing wire bonding on the metal pads it was observed that often the gold pads would peel off instead of forming a bond where the wire bond was applied. The pads would peel off even for weak bond parameters until they were so weak that the gold wire would not stick at all.

The first problem which was identified, was the method of sticking the sample on the Printed Circuit Board (PCB). On the first samples a carbon double–sided adhesive tape was used to fasten the sample. The problem with this tape is that it is relatively thick and soft. The tape absorbs much of the pressure and vibration from the wire bonder causing the bonding process to fail. Another adhesive tape was also tried, a double sided scotch. This tape seemed slightly better, but still not good enough. For the rest of the samples silver paste was used. When this paste is cured is it stiff and keeps the sample in place during bonding. However, the bonding process was still not successful.

Among the failing samples, an interesting property was found. On the same sample there were always some pads which were 'good quality', meaning that a bond could be made with a wide range of bond parameters. Other pads where 'bad quality'. Metal would rip off even with extremely weak parameters. The number of bad contacts and their positions on the sample, varied across samples.

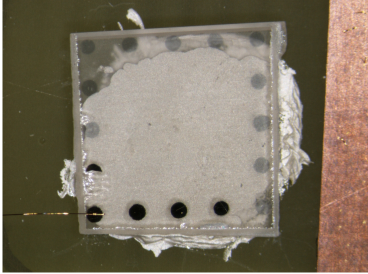

(a) Sample with 20nm/100nm Ti/Au. The Ti is still present, but several of the gold pads peeled off in the ultrasonic bath. Bonding only worked on 1 of the remaining contacts.

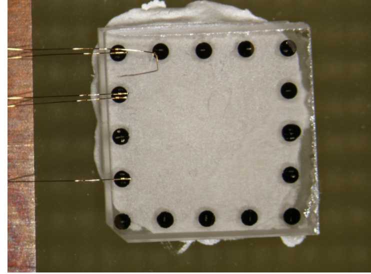

(b) Sample with 20nm/100nm Cr/Au after ultrasonic bath and bonding. Bonding only worked on 4 of the pads.

Figure 15: Samples after ultrasonic bath and wire bonding

A possible cause is that the evaporation process causes the pads to have different adhesion. After a failed bonding attempt, a sample was put in an ultrasonic bath. The 'bad quality' pads where all quickly removed (< 10s) by the ultrasonic energy, while the 'good quality' pads all remained, even after 5min in the bath. A second sample was put in an ultrasonic bath for 5min just after having deposited the pads. For this sample, two pads where completely removed while 4 others lost some of their area. The rest of the pads where unchanged. The subsequent bonding, shown in Figure 14(b) to the remaining pads were all successful.

One possible explanation is that the material flux during evaporation is not uniform across the sample surface. Until the evaporation process was investigated as a possible cause for the bad quality pads, the substrate had always been kept fixed during metal deposition. The electron–beam evaporator has the possibility to rotate the sample during deposition and this function was used for the subsequent samples. Nevertheless, the following samples had the same problems as before.

Further investigation with a thicker (20nm) Ti layer revealed that after ultrasonic bath only the gold pads peeled off — the Ti was still present on the surface, see Figure 15(a). On this sample however, bonding was only successful on one of the remaining pads.

Since the problem seemed to stem from bad Ti/Au adhesion another adhe-

sion layer, chromium, was tried out. A sample with 20nm Cr followed by 100nm Au was put in a ultrasonic bath for 5min. On this sample all pads remained afterwards. However, when trying to perform wire bonding, the metal again peeled off. Bonding was only successful for three pads as can be seen in Figure 15(b).

Scalpel method As a consequence of the problems with the wire bonder method, most of the contacts were made with the scalpel method.

Evaluation of the γ parameter show that the contacts perform well. The distribution of the γ parameter for all contacts prepared with the scalpel method is shown in Figure 16(a). 87.5% of the measurements deviate less than 1% when switching current directions.

Also the δ parameter also looks tolerably good, the majority of data points are below 5%. Moreover, the data points with a high δ parameter generally belongs to high–resistance samples, as seen in Figure 17. For all samples with a sheet resistance less than 300k$\Omega/\square$, the δ parameter is below 5%.

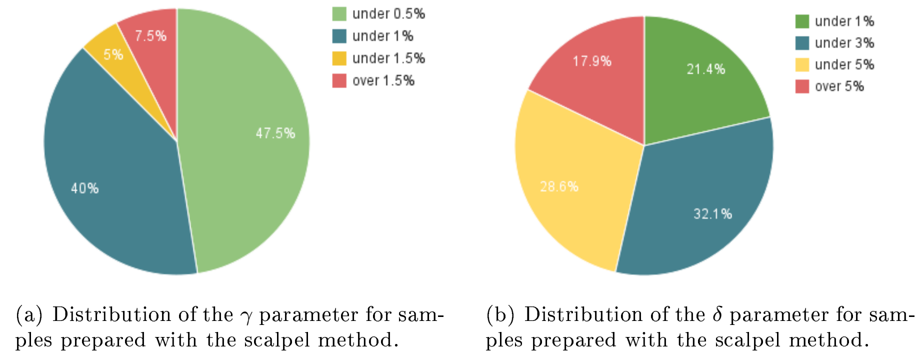

(a) Distribution of the γ parameter for samples prepared with the scalpel method.

(b) Distribution of the δ parameter for samples prepared with the scalpel method.

Figure 16: Distributions of the γ and δ parameters.

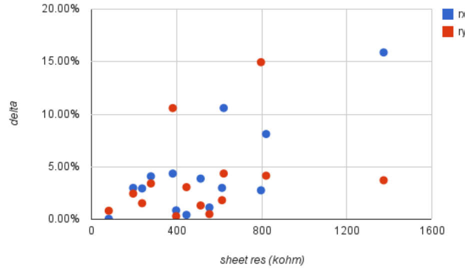

Figure 17: The δ parameter as a function of sheet resistance

4.2 Sheet resistance and the effect of growth parameters

Table 7: Common deposition conditions

Series	Pressure	Fluence	Distance	Off–axis	Temp
Pressure	-	1.79 J/cm^2	45 mm	0°	568–634°C
Fluence	10^{-3} mbar	-	45 mm	0°	628–687°C
Distance	10^{-3} mbar	1.43 J/cm^2	-	0°	670–678°C
Off–axis	10^{-3} mbar	1.43 J/cm^2	45 mm	-	661–683°C
Temp	10^{-2} mbar	1.79 J/cm^2	45 mm	0°	-

All films above 4 u.c. show conductive behaviour, while it was verified that the conductivity disappeared for a sample with 3 u.c. LAO thickness, see Figure 19.

In the series shown here, one parameter has been varied while the other are kept constant. The common parameters for each series can be found in Table 7.

Oxygen pressure In Figure 18(a) the sheet resistance of 3 samples, where the oxygen pressure during growth has been changed. 10^{-3} mbar was found to give the lowest sheet resistance.

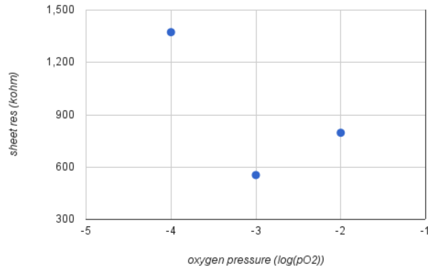

(a) Sheet resistance vs oxygen pressure during growth

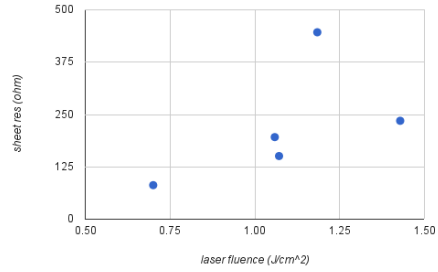

(b) Sheet resistance as a function of laser fluence

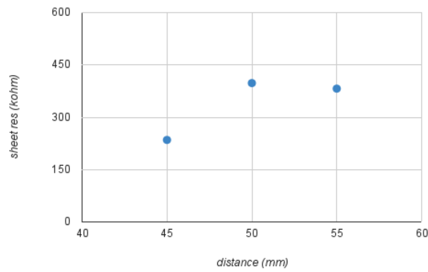

(c) Sheet resistance for samples grown with different substrate–target distance

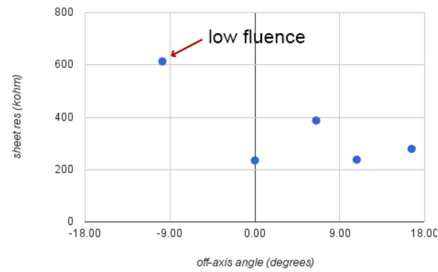

(d) Sheet resistance for samples grown with off–axis PLD

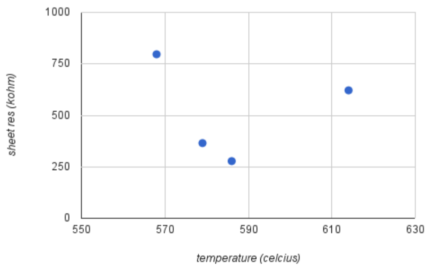

(e) Sheet resistance as a function of substrate temperature

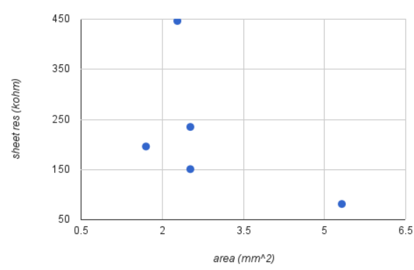

(f) Laser fluence series plotted as a function of laser spot size

Figure 18: Sheet resistance vs growth parameters

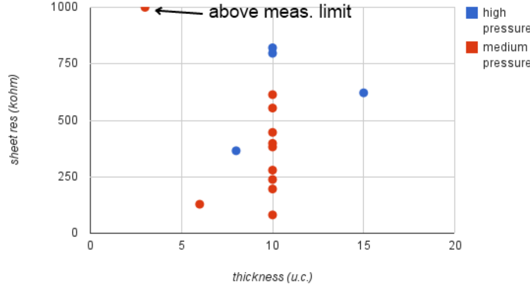

Figure 19: Sheet resistance measurements plotted as a function of film thickness. Most films are grown at 10 u.c. High pressure corresponds to samples grown at 10^{-2} mbar, while medium pressure means 10^{-3} mbar.

Laser fluence The sheet resistances for the laser fluence series are plotted in Figure 18(b). The sheet resistance seem to go down as the fluence is lowered. In fact, the data point at 0.7J/cm^2 is the lowest sheet resistance measured on any of the samples.

Another interesting point about this is that the spot size, the area on the target surface which is hit by the laser pulse, was significantly larger than for the rest of the samples. On this sample the area was 5.3mm^2. For for all the other series the area have been 2.5mm^2, but as the laser mask size have been changed to vary the laser fluence, the spot size changes as well[5]. In Figure 18(f) the data points for this series have been plotted as a function of spot size instead of laser fluence.

Substrate–target distance The results obtained by changing the substrate–target distance are plotted in Figure 18(c). The shortest distance, 45mm, is clearly favorable compared to the longer ones. However, the change from 50 to 55 mm is very small.

Off–axis angle Sheet resistance for samples grown with different off–axis angle is shown in Figure Figure 18(d). The angle does impact the sheet resistance. However no angle different from zero was found to be preferable than the on–axis configuration. The single data point at a negative off–axis angle, was grown with a lower laser fluence than the rest of the samples. For this sample the fluence was 1.18 J/cm^2, while the rest was grown at 1.43 J/cm^2.

[5]The spot size is taken into account when measuring the laser fluence according to Eq (1).

Substrate temperature Samples grown at different substrate temperature are plotted in Figure 18(e). The plot shows a minimum sheet resistance around 600°C .

4.3 Anisotropic resistance

In the same manner as in [11] it was found that the sheet resistance has a significant direction dependence. The resistance values obtained from the van der Pauw method is plotted as functions of terrace widths and step angles, obtained from AFM images, in Figure 20.

The data points in Figure 20 are color coded to indicate which series it belong to. The data point shown in green corresponds to a sample where the substrate itself is conductive. This sample was cooled down in an oxygen pressure of 10^{-7} mbar, and have because of this, significant oxygen vacancies. The two samples marked with purple have both been grown in high pressure (10^{-2} mbar). Not all samples from the previous series have been included here. This is due to lack of aligned AFM data for these samples.

The plotted data include the sheet resistance, $R_\square$, the resistance measured along the x–axis, R_x, and the ratio R_x/R_y. Refer to Figure 10 and Eq (4) for a description of the parameters.

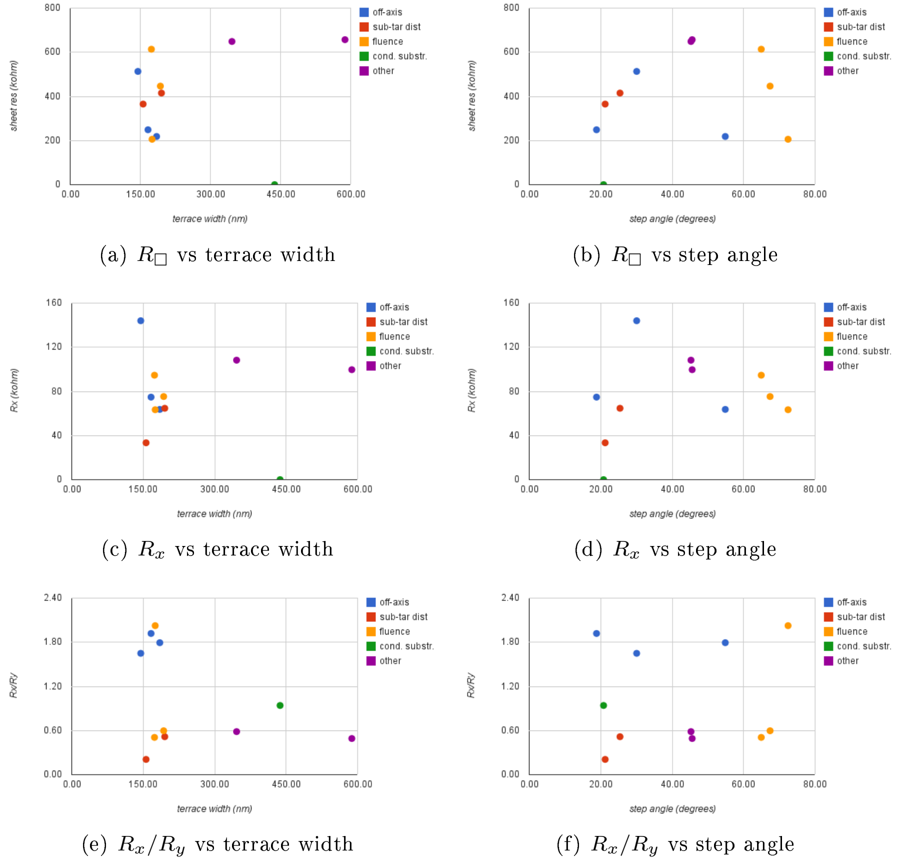

(a) $R_\square$ vs terrace width

(b) $R_\square$ vs step angle

(c) R_x vs terrace width

(d) R_x vs step angle

(e) R_x/R_y vs terrace width

(f) R_x/R_y vs step angle

Figure 20: Sheet resistance measurements plotted as functions of the step angle and terrace width

5 Discussion

5.1 Contacts

The scalpel method have been used with success earlier. However, the desire to have a reproducible contact pattern and well–defined process led to the pursuit of optimizing the wire bond method.

The wire bonder method has several features which make it attractive compared to the scalpel method. A shadow mask is used to pattern the metal. The same pattern is thus transferred to all samples and varying distances between contacts is no longer a problem. Moreover, the contact area[6] can be controlled by using the bond parameters (ultrasonic energy, bond time, temperature and pressure). The wire bonded contacts are smaller than the scalpel scratched trenches and the size is reproducible. Smaller contacts leads to better accuracy in both TLMs and van der Pauw measurements. However, smaller contacts also mean higher contact resistance because contact area is reduced.

One issue with the wire bonder method for this particular application is that the metal film is thin, only about 100nm. This makes bonding harder because there is less material the gold wire can attach to. The film has to be thin however, because the bond should go through both the metal and LAO film and reach the interface. Too thick film would result in a process where the wire bond did not reach the interface at all.

A successful wire bonding process was not achieved. The results indicate that the poor adhesion between Ti and Au from the evaporation process is the main problem. The ultrasonic bath test supports the assumption made from the wire bonder tests: there seems to be a significant difference in quality of the metal pads, even on the same sample. The reason for this is still unanswered. Even when the sample holder was rotated during evaporation, thus removing any effect of non–uniform flux from the evaporation process, the metal pads on the same sample still have varying quality.

The contacts were initially characterized as 'bad' or 'good', by the result of the bonding process. Furthermore, the ultrasonic bath test initially seemed to be able to differentiate the two. Figure 14(b) shows a sample were all the remaining metal pads were good enough to successfully bond to. However, further tests indicated that the picture is not that simple. Both samples in Figure 15 have first been through an ultrasonic bath followed by bonding. As can be seen, the bonding on these samples were not successful on all the remaining pads.

[6] the area of the metal which is in contact with the 2DEG

Chromium did seem to provide better adhesion than titanium and this could be investigated further. However, since the metal still peeled off during bonding, a better alternative is probably to investigate another deposition technique (e.g. sputtering).

The type of metal will also influence the resistance. Schottky barriers often occur at the interface between semiconductors and metals and this depends on the metal–semiconductor work function. Almost all of the contacts are made from a thin (10nm) layer of Ti followed by a thicker gold layer (100nm). This provided good enough contacts for performing the sheet resistance measurements. However, the contact resistances have not been measured due to lack of TLM contact patterns.

The reliable method, scalpel scratching, was used to investigate the sheet resistance of LAO/STO interfaces. The size of these contacts are large, the contact trenches can be up to 1mm long. The variations in structure and size are also large, as a result of the manual method used create them. Trenches are scratched with a scalpel and the mask is made by placing strips of scotch tape across the sample. The contact resistance is expected to vary as a result of this, but since no TLMs are possible on the sample, this can not be investigated.

Contact resistance should not affect sheet resistance measurements, as the van der Pauw method is designed to ignore the contact resistance. However, the size of the contacts could have an impact. In the theoretical derivation of van der Pauw, the contacts have an infinitesimal size and are positioned exactly at the corner of the sample [28]. The scalpel prepared contacts have a non–negligible size compared to the sample and also an ill–defined structure.

When investigating the sheet resistance measurements however, the influence of the contacts are small. Changing direction of the current produced only small variations in the measured values. The distribution shown in Figure 16(a) indicate that the deviations are generally less than 1%. Part of this deviation is also due to the measurement equipment (current source and voltmeter). In addition, Figure 16(b) show that most measurements on parallel sides of the sample give similar results. The deviations were found to generally be less than 5%. Based on this, it is concluded that the influence of contacts on the measurements are small.

5.2 Influence of growth parameters

On most of the samples prepared for this report, the sheet resistance was significantly higher than reported values in literature. The expected value at room

temperature is $\sim 10^4\Omega/\Box$, while almost all our samples displayed sheet resistances above $10^5\Omega/\Box$.

When exploring the growth parameter space, the main focus is to identify which parameters that can significantly lower the sheet resistance.

The optimal oxygen pressure was found to be 10^{-3} mbar. This is contradictory to what other authors report. The reported sheet resistances always goes down when lowering the oxygen pressure. The reason is that more oxygen vacancies are created at lower pressures. However, the oxygen pressure series was grown with a relative high laser fluence. One reason may be that the low pressure (10^{-4} mbar) and high laser fluence resulted in ablated species with too high kinetic energy. In this scenario the surface is damaged during the deposition and the result is a rough interface.

The off–axis angle affected the sheet resistance. However, no off–axis angle produced a lower sheet resistance compared to $\theta = 0°$. The result is also largely asymmetric, a negative off–axis angle resulted in a much larger sheet resistance than the same positive angle. The sample at a negative angle did have a different laser fluence than the rest of the sample. However, the fluence was *lower* than the rest which should result in a lower resistance (as deducted from the laser fluence series). It is likely that the high resistance observed for this sample, is a result of the geometry. Referring to Figure 5, a negative off–axis angle means the ablated species are more affected by the laser pulse than those at a positive angle.

The substrate–target distance was found to yield the best results at the closest position. It is possible to go even closer with our PLD system and this should be investigated further.

With respect to the laser fluence, it was found that lower values produced better interfaces. In fact, the lowest sheet resistance obtained during this project was found during investigation of the laser fluence. For this sample a laser fluence of 0.7J/cm^2 was used and the sheet resistance was $81.2\text{k}\Omega/\Box$.

It is still not clear whether it is the laser fluence or the area of impact that have the greatest impact, but the results indicate that both lowering the fluence and increasing the area reduces the sheet resistance.

The substrate temperature series had a minimum at $\sim 600°$C . In this series of samples also the film thickness varied. However, the thickness should not affect the sheet resistance, according to other authors [30]. A problem with this series is that it was only done up to 614°C whereas several of the other series have been grown at temperatures above this, see Table 7. Thus the effect of substrate temperature on these samples is uncertain.

All the series have a certain spread in temperature between the samples.

The substrate temperature is the most difficult parameter to keep constant. To set the temperature in our system, a setpoint temperature is entered into the controller. The controller is then responsible to ramp up the current and voltage until the setpoint is reached. However, different temperatures are measured with the pyrometer for equal setpoint values. Furthermore, the temperature is not constant. The temperature before and after growth is always somewhat different.

Figure 18(e) indicates that even small differences in substrate temperature can have a significant impact on the interface. When growing new films, care should be taken to keep the temperature as constant as possible between samples.

5.3 Anisotropic resistance

A strong directionality in the sheet resistance is found for all samples. The observation that $R_x \neq R_y$ while $R_{x1} \approx R_{x2}$ is taken as evidence that the directionality is an inherent property of the sheet resistance and not an artifact of the contacts.

By intuition the direction dependence could be related to the step–and-terrace structure of the interface. Since the charge carriers are located at the interface they will come in contact with the steps. A reasonable assumption would be that a certain resistance was associated with each step. If this is the case, the resistance would increase linearly with the number of steps each electron as to cross. The relation can of course be much more complex than this. However, if there is a relation some trends should be visible. More specifically the resistance should be higher for samples with a small terrace width (large density of steps) and a correlation with the step angle relative to the current direction should be visible. If steps are aligned with the current direction (the electrons have to cross only few step edges) the resistance should be lower than if the steps are misaligned or even normal to the current direction.

However, comparing the resistance measurements with AFM data provides no obvious correlation. If the simple model described above was valid, the value of R_x/R_y should be strictly increasing as a function of the step angle (between $0°$ and $90°$). Moreover, $R_x/R_y = 1$ should occur at $45°$. As seen from Figure 20(f), this is clearly not the case. Thus, only speculation about the cause can be done at this point.

It is interesting that the sample with a conducting bulk also displays a large directionality. This sample has a lot of oxygen vacancies and a high conductivity. As stated in Section 2.3.4, oxygen vacancies in STO tend to cluster. It is possible

that oxygen vacancy clustering can account for the observed anisotropy in $R_\square$. It should then be expected that the anisotropy would be less pronounced in high pressure samples, where less oxygen vacancies are present. This was not observed for our samples. However, the high pressure samples was all prepared with a high laser fluence. If indeed this fluence is too high and causes damage to the substrate surface by high–energy LAO species, the conductivity is probably still due to oxygen vacancies. To investigate this further, high pressure samples should be grown with low laser fluence.

6 Conclusion

Conductive LAO/STO interfaces have been demonstrated by PLD growth. They also obey the critical thickness of 4 u.c. The growth have been optimized with the goal of reducing the sheet resistance. The lowest obtained sheet resistance is 81.2k$\Omega/\Box$. The results indicate that to achieve even lower sheet resistances the fluence should be farther decreased, preferably by making the laser spot size larger.

The observed direction dependent conductivity has been compared to AFM data to investigate a correlation with the step–and–terrace topography. However, no correlation is found with the terrace width nor the step angle. Since this directionality is also observed in a sample where the substrate is conductive (by means of oxygen vacancies), this may be a bulk effect.

Attempts at developing a contact creation process using the wire bonder was unsuccessful. The main problem was identified as bad adhesion between Ti and Au. Thus, in order to get further with this method, the metallization process should be changed, e.g. using a sputter instead of the electron–beam evaporator.

A Matlab scripts

```
1
  % Van der Pauw sheet resistance calculation
3 % Data file is two columns: current and voltage
  % Two lines are recorded (positive and negative
5 % input current) for each rotation of the sample
  % Sample is rotated 4 times to measure every
7 % combination

9 % Configuration
  sample = 'p10516';
11 date = '1306'; % mmdd

13 disp(['Van der Pauw measurements for ' sample]);

15 datafile = load(['vanderpauw-', sample, '-', date, '.txt']);

17 Rx1 = (datafile(1,2) / datafile(1,1) + datafile(2,2) / datafile
      (2,1)) / 2
   Rx2 = (datafile(5,2) / datafile(5,1) + datafile(6,2) / datafile
      (6,1)) / 2
19 Ry1 = (datafile(3,2) / datafile(3,1) + datafile(4,2) / datafile
      (4,1)) / 2
   Ry2 = (datafile(7,2) / datafile(7,1) + datafile(8,2) / datafile
      (8,1)) / 2
21

23 Rx = (Rx1 + Rx2) / 2
   Ry = (Ry1 + Ry2) / 2
25

27 pauwfunc = inline(strcat('exp(-pi * ', num2str(Ry), ' / Rs) + exp(-
      pi * ', num2str(Rx), ' / Rs) - 1'), 'Rs');

29 sheet_resistance = fzero(pauwfunc, (Ry + Rx)/2 * pi / log(2));

31 display(sheet_resistance);
```

Listing 1: vanderpauw.m

References

[1] M. Huijben, A. Brinkman, G. Koster, G. Rijnders, H. Hilgenkamp, and D. H. A. Blank, "Structure-Property Relation of SrTiO 3 /LaAlO 3 Interfaces," *Advanced Materials*, vol. 21, pp. 1665–1677, May 2009.

[2] S. A. Chambers, M. H. Engelhard, V. Shutthanandan, Z. Zhu, T. C. Droubay, L. Qiao, P. V. Sushko, T. Feng, H. D. Lee, and T. Gustafsson, "Instability, intermixing and electronic structure at the epitaxial LaAlO3/SrTiO3(001) heterojunction," *Surface Science Reports*, vol. 65, pp. 317–352, Oct. 2010.

[3] H. Kroemer, "Nobel Lecture."

[4] R. Ramesh, "Theory leads the way to new devices," *Nature Nanotechnology*, vol. 3, no. January, 2008.

[5] J. Mannhart and D. G. Schlom, "Oxide interfaces–an opportunity for electronics.," *Science (New York, N.Y.)*, vol. 327, pp. 1607–11, Mar. 2010.

[6] A. Ohtomo and H. Y. Hwang, "A high-mobility electron gas at the LaAlO3/SrTiO3 heterointerface.," *Nature*, vol. 427, pp. 423–6, Jan. 2004.

[7] A. Brinkman, M. Huijben, M. van Zalk, J. Huijben, U. Zeitler, J. C. Maan, W. G. van der Wiel, G. Rijnders, D. H. a. Blank, and H. Hilgenkamp, "Magnetic effects at the interface between non-magnetic oxides.," *Nature materials*, vol. 6, pp. 493–6, July 2007.

[8] N. Reyren, S. Thiel, A. D. Caviglia, L. F. Kourkoutis, G. Hammerl, C. Richter, C. W. Schneider, T. Kopp, A.-S. Rüetschi, D. Jaccard, M. Gabay, D. a. Muller, J.-M. Triscone, and J. Mannhart, "Superconducting interfaces between insulating oxides.," *Science (New York, N.Y.)*, vol. 317, pp. 1196–9, Aug. 2007.

[9] D. P. Norton, *Pulsed Laser Deposition of Complex Materials: Progress Towards Applications*, p. 3. John Wiley & Sons, Inc., 2007.

[10] A. Kalabukhov, R. Gunnarsson, J. Börjesson, E. Olsson, T. Claeson, and D. Winkler, "Effect of oxygen vacancies in the SrTiO3 substrate on the electrical properties of the LaAlO3/SrTiO3 interface," *Physical Review B*, vol. 75, pp. 2–5, Mar. 2007.

[11] F. Dovland, "Contacting the conductive LaAlO 3 / SrTiO 3 interface," tech. rep., NTNU, 2010.

[12] B. G. Streetman and S. K. Banerjee, *Solid State Electronic Devices (Sixth Edtioion).* Pearson Prentice Hall, 2010.

[13] A. Kalabukhov, Y. Boikov, I. Serenkov, V. Sakharov, V. Popok, R. Gunnarsson, J. Börjesson, N. Ljustina, E. Olsson, D. Winkler, and T. Claeson, "Cationic Disorder and Phase Segregation in LaAlO3/SrTiO3 Heterointerfaces Evidenced by Medium-Energy Ion Spectroscopy," *Physical Review Letters*, vol. 103, pp. 3–6, Sept. 2009.

[14] N. Nakagawa, H. Y. Hwang, and D. A. Muller, "Why some interfaces cannot be sharp," *Nature Materials*, vol. 5, pp. 204–209, Jan. 2006.

[15] P. Willmott, S. Pauli, R. Herger, C. Schlepütz, D. Martoccia, B. Patterson, B. Delley, R. Clarke, D. Kumah, C. Cionca, and Y. Yacoby, "Structural Basis for the Conducting Interface between LaAlO3 and SrTiO3," *Physical Review Letters*, vol. 99, pp. 1–4, Oct. 2007.

[16] A. D. McNaught and A. Wilkinson, *IUPAC. Compendium of Chemical Terminology, 2nd ed. (the "Gold Book").* Blackwell Scientific Publications, Oxford, 1997.

[17] S. P. Thiel, *Study of Interface Properties.* PhD thesis, Universität Augsburg, 2009.

[18] L. Qiao, T. Droubay, T. Varga, M. Bowden, V. Shutthanandan, Z. Zhu, T. Kaspar, and S. Chambers, "Epitaxial growth, structure, and intermixing at the LaAlO_{3}/SrTiO_{3} interface as the film stoichiometry is varied," *Physical Review B*, vol. 83, pp. 1–10, Feb. 2011.

[19] Y. Segal, J. H. Ngai, J. W. Reiner, F. J. Walker, and C. H. Ahn, "X-ray photoemission studies of the metal-insulator transition in LaAlO3/SrTiO3 structures grown by molecular beam epitaxy," *Physical Review B*, vol. 80, pp. 4–7, Dec. 2009.

[20] A. Kalabukhov, Y. A. Boikov, I. T. Serenkov, V. I. Sakharov, J. Börjesson, N. Ljustina, E. Olsson, D. Winkler, and T. Claeson, "Improved cationic stoichiometry and insulating behavior at the interface of LaAlO 3 /SrTiO 3 formed at high oxygen pressure during pulsed-laser deposition," *EPL (Europhysics Letters)*, vol. 93, p. 37001, Feb. 2011.

[21] Y. Aiura, "Ultraviolet photoemission study of Sr1-xLaxTiO3," *Journal of Electron Spectroscopy and Related Phenomena*, vol. 78, pp. 199–202, May 1996.

[22] D. D. Cuong, B. Lee, K. M. Choi, H.-S. Ahn, S. Han, and J. Lee, "Oxygen vacancy clustering and electron localization in oxygen-deficient SrTiO(3): LDA + U study.," Mar. 2007.

[23] D. Cuong, "Oxygen vacancies in SrTiO3," *2008 17th IEEE International Symposium on the Applications of Ferroelectrics*, pp. 1–2, Feb. 2008.

[24] L. Qiao, T. C. Droubay, V. Shutthanandan, Z. Zhu, P. V. Sushko, and S. a. Chambers, "Thermodynamic instability at the stoichiometric LaAlO 3 / SrTiO 3 (001) interface," *Journal of Physics: Condensed Matter*, vol. 22, p. 312201, Aug. 2010.

[25] Y. Xie, C. Bell, Y. Hikita, and H. Y. Hwang, "Tuning the electron gas at an oxide heterointerface via free surface charges.," *Advanced materials (Deerfield Beach, Fla.)*, vol. 23, pp. 1744–7, Apr. 2011.

[26] National Science Foundation, "Atomic Force Microscopy."

[27] Digital Instruments Veeco Metrology Group, "MultiMode ™ SPM Instruction Manual," 1996.

[28] L. J. van der Pauw, "A Method of Measuring the Resistivity and Hall Coefficient on Lamellae of Arbitrary Shape," *Philips Technical Review*, vol. 20, p. 220, 1959.

[29] G. Rijnders and D. H. A. Blank, *In Situ Diagnostics by High-Pressure RHEED During PLD*, p. 85. John Wiley & Sons, Inc., 2007.

[30] S. Thiel, G. Hammerl, a. Schmehl, C. W. Schneider, and J. Mannhart, "Tunable quasi-two-dimensional electron gases in oxide heterostructures.," *Science (New York, N.Y.)*, vol. 313, pp. 1942–5, Sept. 2006.